**Proceedings Paper:**
Doychinov, V orcid.org/0000-0001-6730-0057, Russell, C orcid.org/0000-0002-7322-8255, Somjit, N orcid.org/0000-0003-1981-2618 et al. (3 more authors) (2019) Investigation of Implantable Antennas for Exploratory Neuroscience Studies. In: Proceedings of the Loughborough Antennas & Propagation Conference 2018. Loughborough Antennas & Propagation Conference 2018 (LAPC 2018), 12-13 Nov 2018, Loughborough, UK. Institution of Engineering and Technology . ISBN 978-1-78561-969-4

https://doi.org/10.1049/cp.2018.1445

# Investigation of Implantable Antennas for Exploratory Neuroscience Studies

*V Doychinov*[*,‡], *C Russell*[*], *N Somjit*[*], *I D Robertson*[*], *S Chakrabarty*[†], *D P Steenson*[*]

[*] *School of Electronic and Electrical Engineering, University of Leeds, Leeds, United Kingdom,*
[†] *Faculty of Biological Sciences, University of Leeds, Leeds, United Kingdom,*
[‡] *v.o.doychinov@leeds.ac.uk*

**Keywords:** Implantable, Antenna, Neuroscience, Lightweight, Compact

## Abstract

In this paper we present a thorough and rigorous characterisation of the dielectric properties of rat skin tissue, including statistical processing. This data is used for a proof of concept study of the design, fabrication, and measurement of lightweight, flexible, and conformable microstrip patch antennas, to later enable improved chronic neuroscience research studies.

## 1 Introduction

The average age of the population of both the United Kingdom and the world is rapidly increasing, and this characteristic has been identified by numerous international bodies as a global issue. This ageing, among other things, has resulted in an increased demand for therapies for age-related neurological conditions such as Parkinson's disease and Alzheimer's disease [1, 2]. This in turn has driven a surge in neuroscience and medical research into electroceutical therapies to monitor and control these diseases to maintain and improve the quality of life of the affected patients.

Traditionally, small animals such as rats are used during the exploratory and pre-clinical stages of these neuroscience research studies, which has predominantly focused on recording and stimulating nerve signals [1]. The recording and stimulation is achieved via implantable electronics, conventionally requiring an electrical transcutaneous tether to provide power and communication capabilities [3]. This tether can restrict the movement of the animals, potentially distressing them, whilst also creating uncertainties in chronic behavioural studies in neurophysiology [4]. Removing the tethering in favour of batteries mitigates these issues, as well as decreasing the risk of infection, but at a cost of limiting the study to a short time period and increasing the mass and volume of the implant [5].

A better proposal is the use of simultaneous wireless information and power transfer (SWIPT) which would allow the technology to be powered for the duration of the study and when suitably designed, will not exhibit a foreign body response in the animal. This further removes any surgical intervention and its associated risks of infection to modify the operating parameters of the technology or to replenish its power source(s). SWIPT has been demonstrated for implantable and wearable technologies which is commonly achieved via inductive coupling, confining the animal or patient to an area within the reach of the primary coil [6]. This approach is limited when translated into a practical clinical setting as the movements of the animal or patient will be constrained by the short operating distance of an inductive wireless power transfer (WPT) link.

Moving from near-field SWIPT to far-field SWIPT would facilitate these studies even further. Currently, implantable RF antennas operate in frequency bands such as the Medical Implant Communication System (MICS, 403 MHz) [7, 8] and the Industrial, Scientific, and Medical bands (ISM; 433 MHz, 2.45 GHz, 5.8 GHz, and 24.125 GHz) [8]. To improve energy efficiency and use, dual-band antennas working at the MICS and ISM bands are often used to enable novel Wake-Up Receiver (WUR) approaches [9]. These have been demonstrated in academic research papers in the past for implantable electronic aimed at humans. This has been facilitated by widely-available data on the dielectric properties of various human tissues [9, 10].

However, translating these to neuroscience and neurophysiology animal studies is not without significant challenges. For one, implantable electronics are conventionally fabricated using thick rigid substrates which will restrict the movement of the animal, unless they are miniaturised, complicating the overall design. Furthermore, air pockets between the skin and the antenna have been shown to be detrimental to the antenna performance [11]. The large volume and mass of these implants has also been demonstrated to affect the behaviour of the animals. Finally, statistically sound data on the dielectric properties of rat tissues, which can be used for antenna design purposes, is not readily available in the literature [8].

In this work, we utilise an accepted method of characterising the dielectric properties of biological tissues to measure skin tissue samples from female Sprague-Dawley rats and to provide data that has been statistically evaluated from a biological perspective to scrutinise the inherent biological variance

and its influence on the high-frequency dielectric properties. These statistical evaluations of the tissue are then utilised in industry-standard 3D EM simulation software, Ansys HFSS. We demonstrate the usefulness of this data via the design of microstrip patch antennas on thin, flexible, and conformable polyimide substrate. The aim of this is to reduce the physical presence of future implantable technology in the animal by allowing the antenna to conform to the ever-changing organic shape of its body. This in turn will promote natural animal behaviour and enhance neuroscience research. *Ex-vivo* measurements of these antennas show potential for power and data transfer from beneath the skin of rats to be used for exploratory and pre-clinical research.

## 2 Biological Tissue $\dot{\epsilon_r}$ Measurements

Since the intended application for the antennas presented in this work is to be used in subcutaneous implants, measurements of the complex relative permittivity $\dot{\epsilon_r} = \epsilon_r' + j\epsilon_r''$ focused on that of skin tissue. A commercially-available dielectric probe kit (Keysight 85070E) together with a FieldFox N9917A Vector Network Analyser (VNA) was used to perform these measurements. The open-ended coaxial dielectric probe is a good choice for measurements of soft biological tissues, provided there is flush contact between the surface of the probe and that of the tissue [12].

### 2.1 Tissue Handling and Processing

The skin samples were removed from female Sprague-Dawley rats, aged 6-8 weeks and weighing 229 $\pm$ 5 g. These were taken following unrelated terminal study measurements for which these antenna designs would be utilised in synonymous future measurements. The skin was cut into 60 mm $\times$ 60 mm squares, and the fur removed to help achieve flush contact between the dielectric probe tip and the tissue. Excess muscle tissue was also removed from the underside of the skin. This was done to better reflect the final implant location, i.e. between the muscle and skin tissues. A photograph of a single skin sample is shown in Fig. 1, after shaving of the fur but prior to $\dot{\epsilon_r}$ measurements.

Following removal in a surgical laboratory, the skin tissue was temporarily stored in oxygenated (95% $O_2$, 5% $CO_2$) Krebs - Henseleit solution (in mmol/l: 117 NaCl, 4.7 KCl, 2.5 $CaCl_2$, 1.2 $MgSO_4$, 24.8 $NaHCO_3$, 1.2 $KH_2PO_4$ and 11.1 glucose), before conducting the measurements. All animal experiments from which the skin are obtained were approved by the University of Leeds Animal Welfare and Ethics Committee, and were conducted in accordance with the UK Animals (Scientific Procedures) Act 1986.

### 2.2 Relative Permittivity Measurement Details

Each skin sample was measured at five different positions consisting of the four corners of the approximately rectangular skin sample and its geometric centre, as illustrated in Fig. 1, with each position measured three times at 30 s intervals. Measuring individual points across a larger sample yields a better statistical representation of the expected variability of the dielectric properties of the tissue with respect to thickness, ambient conditions and general variance within the overall population [13]. In total, eight skin samples were measured, with the tissue thickness of each measurement point measured with digital Vernier callipers and recorded as well.

The VNA used in conjunction with the Keysight 85070E dielectric probe kit was configured to measure 401 points over the frequency range 144 MHz – 18 GHz, with an IFBW of 300 Hz and port output power of -15 dBm.

### 2.3 Measurement Results and Data Processing

Typical results obtained for a single tissue sample are presented in Fig. 2. While variability between subsequent measurements of a single positions is minimal, there is an observable difference between individual positions.

Despite best efforts during dielectric probe measurements, on occasion an air gap was left between the dielectric probe tip and the tissue sample. When that happened, measurement results were heavily skewed towards lower relative permittivity and were classed as outliers and removed from subsequent processing. An example of such outlier measurements is given in Fig. 3.

Once measurements from all samples were collected and outliers removed, descriptive statistics (minimum, maximum, mean, standard deviation) were calculated on a per-frequency point basis using the free and open-source Python library NumPy. These statistics were then used to find the expanded uncertainty and the corresponding 95% confidence interval (CI) of the mean, in accordance with [14], again on a per-frequency point basis. The final results of this statistical analysis are presented in graphical form in Fig. 4.


**Fig. 1:** A single rat skin tissue sample. Crosses denote positions used for dielectric probe measurements.

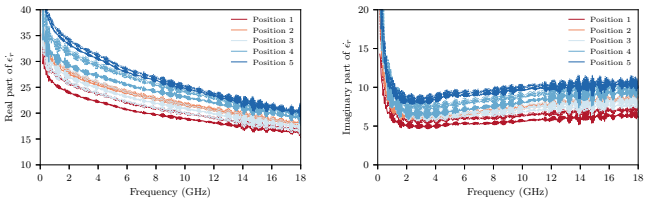


**(a)** Real part $\epsilon_r'$ **(b)** Imaginary part $\epsilon_r''$

**Fig. 2:** Complex relative permittivity measurement results for a single rat skin tissue sample.

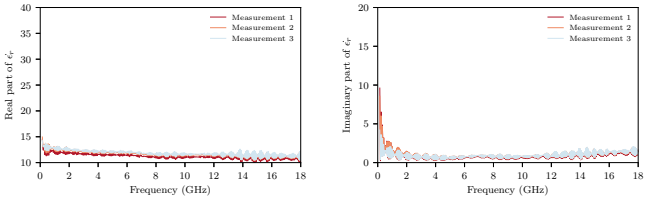


**(a)** Real part $\epsilon_r'$ **(b)** Imaginary part $\epsilon_r''$

**Fig. 3:** Example of outlier results due to an air gap between the dielectric probe tip and the tissue sample. Note: axes are same as those in Fig. 2

In addition, the average thickness of the measured rat skin samples was found to be 1.595 mm with a standard deviation ($\sigma$) of 0.489 mm.

Finally, the obtained means for both the real and imaginary part of the complex relative permittivity of rat skin were exported to files suitable for use in Ansys HFSS. These were then used during the next step, the design and simulation of microstrip patch antennas. One aim for future work is to expand the measurement frequency range and fit the obtained data to a dielectric dispersion model. A graphical representation of the described process is shown in Fig. 5.

## 3 Antenna Design and Fabrication

Several requirements were identified early for the antennas designed and developed as part of this study. First, the antennas have to be flexible and conformable, i.e. they can follow the

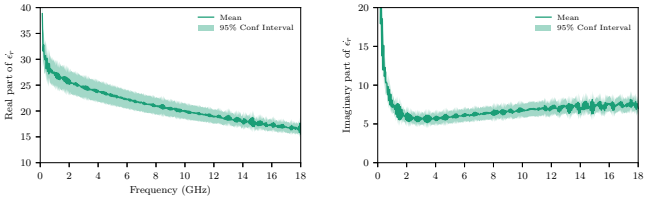


**(a)** Real part $\epsilon_r'$ **(b)** Imaginary part $\epsilon_r''$

**Fig. 4:** Obtained mean and 95% CI of the mean for $\epsilon_r$ of rat skin.

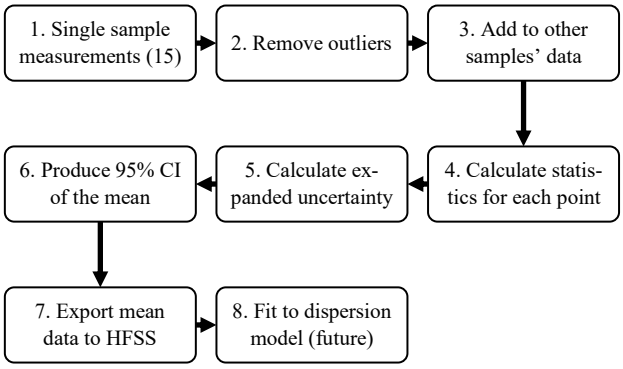


**Fig. 5:** A summary of the data processing flow. The real and imaginary part are processed separately but use the same flow.

organic shape of the animal while being implanted just beneath the skin. This way the antenna will have near-zero-presence, allowing the animal to move without irritation. Furthermore, the mass of the antennas has to be minimal, in any case no more than 10% of the overall mass of the animal, or 20 g in the case of rats [15]. Finally, while no particular frequency band is explicitly targeted, the operating frequency is expected to be in the sub-6 GHz region, due to constraints discussed later, while occupying no more than a 15 mm square.

In the first instance, several variants of a rectangular microstrip patch antennas were investigated, incorporating diagonal and cardinal slits in order to reduce their first resonant frequency [16].

### 3.1 Design and Simulation

For the antenna substrate, polyimide ($\epsilon_r = 3.6$, $\tan\delta = 0.01$) was selected as it has been proven to be biocompatible and has a history of being used for chronic implantable technologies. This material is supplied as sheets of specific thickness, of which $50\,\mu m$ is chosen for this work. This thickness provides excellent flexibility and conformability, however this comes at the cost of radiation efficiency. It has long been established [17] that the radiation efficiency of microstrip patch antennas on thin substrates is low, due to the high $Q$-factor of the resonant cavity formed between the patch and the ground plane.

The starting point, a basic microstrip patch antenna, was designed using the well-established procedure described in [18]. Following that, parametric sweeps of the length and width of the cardinal and diagonal slits were carried out in Ansys HFSS, a commercially available 3D FEM EM simulator, in order to reduce the operating frequency of the antennas to below 6 GHz.

The metal surfaces were modelled as two-sided finite impedance boundaries, with Perfectly-Matched Layers (PML) as radiation boundary. The rat skin tissue was modelled as a

square block with varying thickness, depending on measured data, and frequency-dependent relative permittivity and loss tangent. The latter two were imported following the statistical processing described in the previous Section.

### 3.2 Fabrication

The various microstrip patch antennas were structured on $50\,\mu m$ thick polyimide sheets. Initially, the sheets were spin-coated with $1\,\mu m$ thick S1813 photoresist and cured at $115°\,C$ for 4 minutes before being exposed using laser write technology (Heidelberg Instruments MLA 150) for a total dose of $190\,mJ/cm^2$. The photoresist was then treated with chlorobenzene ($C_6H_5Cl$) for 60 s and developed in MF-319, again for 60 s.

The patterned substrate was micro-roughened using reactive ion etching (100 W, 30 s, 25 sccm $O_2$) to improve the adhesion between the PI and the subsequent coating of metal (Ti:Au, 10:200 nm), which was deposited using electron beam evaporation [19]. A clean lift-off in acetone followed by an isopropanol ($C_3H_8O$) rinse results in the final antenna geometry. The side of the PI sheets that forms the ground plane for the patch antennas was also micro-roughened and metal coated with electron beam evaporated metal (Ti:Au, 10:200 nm).

Miniature Hirose U.FL connectors were used to enable *S*-parameter measurements of the fabricated antennas using a VNA. Due to the thin substrate and metal layers, soldering these connectors was not deemed suitable. Instead, silver-loaded epoxy was used to bond the connectors to the Ti:Au metal layer. Furthermore, a $500\,\mu m$ diameter biopsy punch was used together with a silver epoxy filling to provide metallised via functionality and connect the ground pads of the U.FL connector to the microstrip ground plane. The silver epoxy was cured at room temperature for 24 hours before the antennas were first measured.

A photograph of three of the fabricated antennas, demonstrating the three different designs used, is given in Fig. 6. Even though all fabricated antennas were measured, results are reported here for the diagonal slits version, which showed the closest correlation with simulation results.

## 4 *Ex-Vivo* Antenna Measurement Results

The return loss of the fabricated antennas was measured in a laboratory environment both with and without *ex-vivo* rat skin tissue samples placed on top of them, acting as a superstrate layer. Since the fabricated antennas are physically much smaller than the tissue skin samples used for $\epsilon_r$ measurements, the skin tissue was further divided into smaller pieces, roughly measuring a 40 mm square. These were still large enough to fully cover the Antennas Under Test (AUT), including the U. FL connectors, and emulate implanted conditions. Photographs of these smaller skin pieces are shown in Fig. 7.

The antennas were measured over the same frequency range for which the complex relative permittivity of the rat skin was

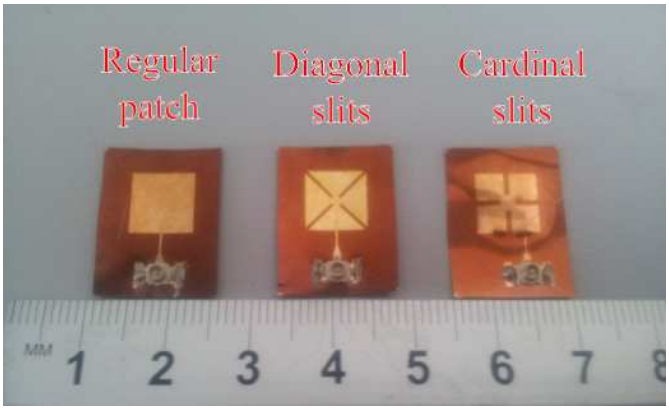


**Fig. 6:** A photograph of a representative sample of fabricated antennas on PI substrate, including epoxy-bonded U.FL connectors.

measured, i.e. 144 MHz – 18 GHz, using the same FieldFox N9917A portable VNA. A single-port mechanical Short-Open-Load (SOL) calibration was used before conducting the measurements. Photographs illustrating the measurement setup in case of free-space conditions and with rat skin tissue placed on top of the antennas are given in Fig. 8 and Fig. 9, respectively. Good contact between the skin tissue and the AUT was ensured by firmly pressing the tissue down with metal tweezers.
The use of U.FL connectors, while necessary due to the small size of the antennas and the thin dielectric and metal layers, presented several measurement challenges. Most important of

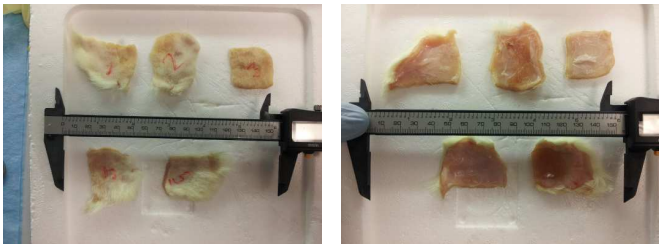

**(a)** Top view **(b)** Upside-down view

**Fig. 7:** Rat skin tissue cut into smaller pieces for antenna return loss measurements.


**(a)** Overview **(b)** AUT close-up

**Fig. 8:** Return loss measurement setup in case of free-space conditions.

these was that U.FL to SMA adapters and short U.FL cables were required to connect the antennas to the SMA interface of the FieldFox VNA. Since the SOL calibration kit used was an SMA one, this meant that the contributions of the adapters and U. FL cables were embedded in the measurement results of the antennas.

To address this, the electrical delay of the adapters and the $S$-parameters of the cables were measured separately and were subsequently de-embedded using $T$-matrix representation and the Python library scikit-rf. An illustration of the effect of this de-embedding is presented in Fig. 10, which also shows a comparison with the simulated return loss obtained from Ansys HFSS. There is a small frequency shift, which is attributed to the parasitics of the silver epoxy bonded U.FL connector, as well as differences in the actual relative permittivity of polyimide to that of the modelled one.

Another challenge is that U.FL connectors and cables are nominally rated up to 6 GHz and for a limited number of mating cycles [20], with performance degrading quickly after that. In addition, the U.FL connectors tended to de-laminate quite easily when disconnecting the U.FL cable from the AUT.

The combination of these factors meant that repeated measurements of the same antenna samples on different days was difficult and sometimes impossible. This is another reason why the rat skin samples that were used for complex relative permittivity measurements were sub-divided into smaller pieces, to enable multiple return loss measurements emulating an implanted antenna while minimising the number of connecting and disconnecting the U.FL cable from the U.FL connector.

To validate the accuracy and usefulness of the obtained complex relative permittivity data for rat skin tissue, the fabricated antennas were measured with rat skin tissue samples that were not measured with the dielectric probe *a priori*. Only the thickness of these news samples was measured and used in the HFSS model. A comparison between the simulated and measured return loss results for one such microstrip patch antenna with diagonal slits is presented in Fig. 11.

It is evident that there is excellent agreement between simulated and measured return loss, when the antenna is in emulated implanted condition, i.e. a rat skin tissue sample is placed on top of the antenna. This shows that the complex relative permittivity data that was gathered, summarised, and exported for use in HFSS is suitable for design purposes.


**(a)** Overview **(b)** AUT close-up

**Fig. 9:** Return loss measurement with tissue placed on top of the microstrip patch antenna.

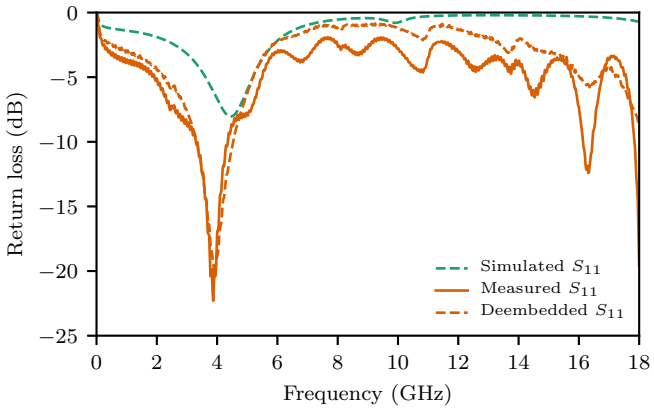


**Fig. 10:** A comparison between simulated and measured return loss for the diagonal slits antenna design. Shown is also the effect of de-embedding the U.FL cable and U.FL to SMA adapters.

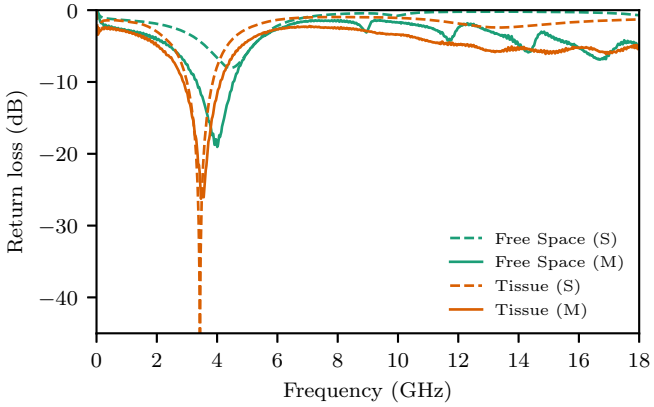


**Fig. 11:** Comparison between simulated (S) and measured (M) return loss for an antenna in free-space condition and in emulated implanted condition.

## 5 Conclusion & Future Work

In this paper, the authors have presented and discussed the characterisation of the dielectric properties of rat skin tissue, together with a brief statistical analysis. This data was subsequently used for the design and fabrication of lightweight, flexible, and conformable antennas on thin polyimide substrate. Measurement results show excellent agreement, validating the quality of the obtained data and the novel fabrication approach.

In future contribution, the authors will expand on the statistical processing and will fit the data to existing dielectric dispersion models. Additional antenna topologies will be studies, as well as the effect of implantation location on the electromagnetic properties of these antennas.

## Acknowledgements

The authors are grateful to Dr Roger Kissane and Dr Philippa Warren for the provided samples of *ex-vivo* rat skin. The authors would also want to thank the Engineering and Physical Sciences Research Council (EPSRC) for their financial support under grants EP/N005686/1 (SWIFT) and EP/M025977/1, as well as the International Foundation for Research in Paraplegia.

## References

[1] Thompson, D.M., Koppes, A.N., Hardy, J.G., Schmidt, C.E.: 'Electrical Stimuli in the Central Nervous System Microenvironment', *Annual Review of Biomedical Engineering*, 2014, **16**, (1), pp. 397–430

[2] Lozano, A.M., Dostrovsky, J., Chen, R., Ashby, P.: 'Deep brain stimulation for Parkinson's disease: disrupting the disruption', *The Lancet Neurology*, 2002, **1**, (4), pp. 225–231

[3] Biran, R., Martin, D.C., Tresco, P.A.: 'The brain tissue response to implanted silicon microelectrode arrays is increased when the device is tethered to the skull', *Journal of Biomedical Materials Research Part A*, 2007, **82A**, (1), pp. 169–178

[4] Wentz, C.T., Bernstein, J.G., Monahan, P., Guerra, A., Rodriguez, A., Boyden, E.S.: 'A wirelessly powered and controlled device for optical neural control of freely-behaving animals', *Journal of Neural Engineering*, 2011, **8**, (4), pp. 046021

[5] Kilinc, E.G., Dehollain, C., Maloberti, F. 'Implantable Monitoring System for Rodents'. (Springer, Cham, 2016. pp. 13–23

[6] Shin, G., Gomez, A.M., Al.Hasani, R., Jeong, Y.R., Kim, J., Xie, Z., et al.: 'Flexible Near-Field Wireless Optoelectronics as Subdermal Implants for Broad Applications in Optogenetics', *Neuron*, 2017, **93**, (3), pp. 509–521.e3

[7] Islam, M.N., Yuce, M.R.: 'Review of Medical Implant Communication System (MICS) band and network', *ICT Express*, 2016, **2**, (4), pp. 188–194

[8] Karacolak, T., Cooper, R., Topsakal, E.: 'Electrical Properties of Rat Skin and Design of Implantable Antennas for Medical Wireless Telemetry', *IEEE Transactions on Antennas and Propagation*, 2009, **57**, (9), pp. 2806–2812

[9] Yoo, H., Cho, Y.: 'Miniaturised dual-band implantable antenna for wireless biotelemetry', *Electronics Letters*, 2016, **52**, (12), pp. 1005–1007

[10] Gabriel, S., Lau, R.W., Gabriel, C.: 'The dielectric properties of biological tissues: II. Measurements in the frequency range 10 Hz to 20 GHz', *Physics in Medicine and Biology*, 1996, **41**, (11), pp. 2251–2269

[11] Karacolak, T., Cooper, R., Butler, J., Fisher, S., Topsakal, E.: 'In Vivo Verification of Implantable Antennas Using Rats as Model Animals', *IEEE Antennas and Wireless Propagation Letters*, 2010, **9**, pp. 334–337

[12] Gregory, A.P., Clarke, R.N., Hodgetts, T.E., Symm, G.T. 'RF and microwave dielectric measurements upon layered materials using coaxial sensors, NPL Report MAT 13'. (NPL, UK, 2008.

[13] Peyman, A., Rezazadeh, A.A., Gabriel, C.: 'Changes in the dielectric properties of rat tissue as a function of age at microwave frequencies', *Physics in Medicine and Biology*, 2001, **46**, (6), pp. 1617–1629

[14] United Kingdom Accreditation Service. 'The Expression of Uncertainty and Confidence in Measurement'. (, 2012. November

[15] Meng, E., Hoang, T.: 'MEMS-enabled implantable drug infusion pumps for laboratory animal research, preclinical, and clinical applications', *Advanced Drug Delivery Reviews*, 2012, **64**, (14), pp. 1628–1638

[16] Wong, K.L.: 'Compact and Broadband Microstrip Antennas'. Wiley Series in Microwave and Optical Engineering. (New York, USA: John Wiley & Sons, Inc., 2002)

[17] Balanis, C.A.: 'Antenna theory: analysis and design'. 4th ed. (Wiley, 2016)

[18] Volakis, J.L.: 'Antenna engineering handbook'. 4th ed. (McGraw-Hill, 2007)

[19] Jackson, N., Keeney, L., Mathewson, A.: 'Flexible-CMOS and biocompatible piezoelectric AlN material for MEMS applications', *Smart Materials and Structures*, 2013, **22**, (11), pp. 115033

[20] 'U.FL series - HIROSE Electric Group'. (, . Available from: `https://www.hirose.com/product/en/products/U.FL/`